氩弧重熔对 Q235 钢热浸镀铝层组织和性能的影响

赵 霞[1], 徐家文[1], 孙永鑫[2]
(1. 黑龙江科技学院 材料科学与工程学院, 哈尔滨 150027;
2. 哈尔滨电机厂有限责任公司 哈尔滨大电机研究所, 哈尔滨 150040)

赵 霞

摘 要: 采用氩弧重熔技术对 Q235 钢热浸镀铝层进行改性处理, 利用扫描电子显微镜和 X 射线衍射仪对重熔前后组织进行了观察, 并测定了重熔前后截面显微硬度, 研究了重熔工艺参数对热浸镀铝层组织和性能的影响. 结果表明, 热浸镀铝层经氩弧重熔处理后, 分层现象消失, 组织上梯度过渡, 试件由重熔层和淬硬层及基体构成. 氩弧重熔处理能明显提高热浸镀铝层的显微硬度. 氩弧重熔工艺参数对重熔层深度、硬度和裂纹率影响较大, 焊接电流增加或焊接速度减小时, 重熔层深度增加, 硬度升高, 裂纹率下降.

关键词: 热浸镀铝; 氩弧重熔; 组织; 显微硬度
中图分类号: TG174.4 文献标识码: A 文章编号: 0253-360X(2009)09-0093-04

0 序 言

热浸镀铝 HDA(hot dipping aluminizing)是继热浸镀锌之后发展起来的一种高效防护技术. 钢材经热浸镀铝后形成了以铝为表面层, 铁铝金属间化合物为过渡层的复合材料[1]. 扩散形成的铁铝金属间化合物具有抗高温氧化、耐磨、硬度高、耐工业介质腐蚀等优点, 性能全面. 另外, 钢材热浸镀铝工艺简单, 获得的镀层厚, 因而, 它是目前最经济的涂覆铝的方法. 近年来热浸镀铝钢材在石油化工、建筑工程、交通运输、海洋工程等领域获得了广泛应用. 但是, 钢材热浸镀铝镀层具有分层现象, 造成了性能上的突变, 并且镀层还有一定脆性, 这都影响热浸镀铝镀层优异性能的发挥. 如何利用钢材热浸镀铝层优异的表面性能, 并降低镀层的脆性, 这在现实生产中具有十分重要的意义.

氩弧重熔是一项成本低、工艺简单、效率高的表面强化技术, 与激光、电子束、等离子束热源相比, 更易于普及. 氩弧重熔后的组织均匀致密、明显细化, 并且重熔层与基体界面为良好的冶金结合[2,3]. 采用氩弧重熔技术对 Q235 钢热浸镀铝层表面进行改性处理, 可以改变浸镀层的形态、组织及元素分布, 达到提高质量的目的.

收稿日期: 2008-07-24
基金项目: 黑龙江省教育厅科学技术研究项目(11511249)

1 试验方法

试验选用熔剂法进行 Q235 钢热浸镀铝. 试样尺寸为 30 mm×30 mm×5 mm, 其工艺流程为除油→除锈→助镀→烘干→铝液浸镀→冷却. 浸镀温度 750 ℃, 保温时间 8 min.

氩弧重熔选用 MW3000 型数字式电焊机, 电弧电压 10 V, 氩气流量为 7 L/min, 焊接电流和焊接速度可调. 试验中, 在保持电弧电压、焊接速度不变的情况下, 考察焊接电流对重熔层深度、组织和性能的影响. 在保持电弧电压、焊接电流不变的情况下, 考察焊接速度对重熔层深度、组织和性能的影响, 并测试不同焊接电流和焊接速度下裂纹率(100 mm 长焊道上裂纹平均数).

利用 MX-2600FE 型扫描电镜及其能谱附件进行组织形貌观察和微区成分鉴定, 利用 D/MAX 型 X 射线衍射仪进行物相鉴定. 采用 MHV2000 型数显显微维氏硬度仪测定氩弧重熔前后试件截面的显微硬度分布.

2 试验结果及讨论分析

2.1 组织分析

2.1.1 热浸镀铝层组织分析

图 1 所示为热浸镀铝层组织形貌, 从图 1 中可以看出, 镀层存在明显的分层现象, 与基体呈冶金结

合. 这是因为浸镀时铁与熔融铝液接触, 相界面浸润、熔化、扩散、生长, 一定时间后便生成一定厚度的金属间化合物层, 即扩散层; 提取试样时, 表层粘附一层铝液. 由此推断, 上层为富铝层, 下层为扩散层, 扩散层形状呈柱状延伸到基体中.

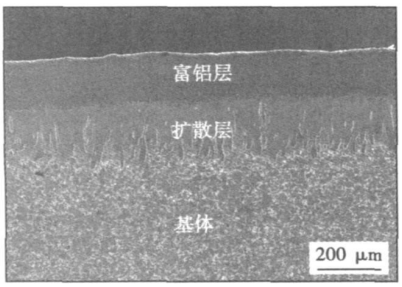

图 1 热浸镀铝层组织形貌

Fig. 1 SEM micrographs microstructure of HDA

为确定热浸镀铝层物相, 对镀层进行 X 射线衍射分析. 经镀层的 X 射线衍射图谱及各衍射峰的标定结果, 可确定镀层中的主要成分为 Al, $FeAl_3$ 和 Fe_2Al_5 三相, 这与文献[4] 的结果一致.

2.1.2 氩弧重熔层组织分析

在热浸镀铝层表面进行氩弧重熔, 其焊接电流 $I=80$ A, 焊接速度 $v=300$ mm/min, 电弧电压 $U=10$ V, 氩弧重熔层组织形貌如图 2 所示, 热浸镀铝层经氩弧重熔处理后, 分层现象消失, 组织梯度过渡, 试件由重熔层和淬硬层及基体构成. 这是因为氩弧的特点是电弧功率密度大, 能量非常集中, 瞬间可将表面的热浸镀铝层与基体表层加热熔化, 形成的熔池温度高达 5 000 ℃, 具有较强的搅拌性, 在极短时间内热浸镀铝层和基体发生相互扩散并达到均匀混合, 使合金元素重新分布, 沿横截面方向出现了组织变化[5, 6].

为确定氩弧重熔层物相, 对其进行X射线衍射分析, 其 XRD 衍射图谱标定如图 3 所示, 经标定认为重熔层由 Al, Fe, Fe_3Al 和 $FeAl_3$ 四相组成. 单相的存在是因氩弧瞬时升温及瞬时冷却的特点, 某些 Fe-Al 化合物还没来得及完全形核、析出, 重熔层即完全凝固, 因而在氩弧重熔后存在 Fe 与 Al 的单相. 淬硬层组织为马氏体+残余奥氏体, 这是因为在熔池固相一侧的基体在氩弧热输入的作用下, 快速形成奥氏体, 由于高温停留时间很短, 奥氏体晶粒来不及长大, 在基体自激冷作用下, 发生马氏体转变.

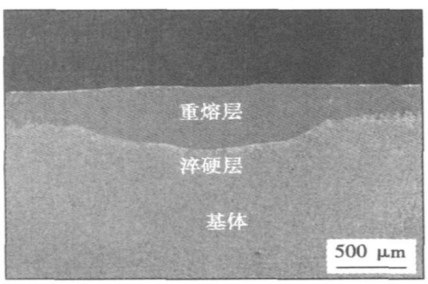

图 2 氩弧重熔层组织形貌

Fig. 2 SEM micrographs microstructure of TIG remelting

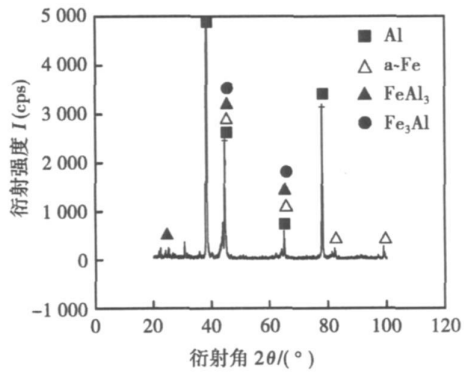

图 3 氩弧重熔层 XRD 图谱

Fig. 3 XRD pattern of TIG remelting coating

图 4 所示为氩弧重熔前后截面线扫描能谱图, 从图中可见, 在重熔层与基体的结合界面上, Al 元素由重熔层到基体呈梯度减小; Fe 元素由重熔层到基体呈梯度增加, 在重熔层内部 Fe 元素含量较重熔前明显增加. 从图中还可见, 因 Fe, Al 元素相互扩散, 在富铝层中有大量 Fe-Al 化合物形成, 并贯穿整个富铝层, 重熔区裂纹清晰可见. 能谱分析表明, 热浸镀铝层氩弧重熔后, 热浸镀铝层与基体在高温下发生了互扩散, 形成了梯度冶金结合层.

2.2 显微硬度分析

图 5 为焊接电流 $I=80$ A, 焊接速度 $v=300$ mm/min, 电弧电压 $U=10$ V 处理热浸镀铝层前后的截面显微硬度变化曲线. 由图可见, 氩弧重熔处理能明显提高热浸镀铝层的显微硬度. 未重熔处理前热浸镀铝试件各层的显微硬度差异较大, 表层硬度较低, 只有 160 HV, 而重熔处理后, 表面硬度可达 620 HV, 重熔层内硬度较均匀; 在淬硬层硬度过渡缓慢, 并随着与表面距离的增加硬度降低, 直至基体. 硬度分布与组织有关. 重熔处理后, 表面富铝层消失, 转变为重熔层, 重熔层成分较均匀且含有 Fe_3Al, $FeAl_3$ 相, 故硬度较高; 淬硬层组织主要为马氏体和残余奥氏体, 故硬度也较高, 但在淬硬层中随着距表

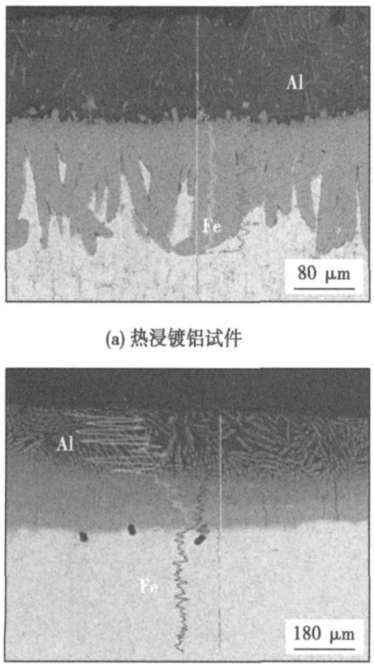

图 4　氩弧重熔前后截面线扫描能谱图

Fig. 4　Line distribution of element on cross-section by TIG remelting pre- and post of HDA

面距离的增加，温度下降，溶入奥氏体的碳含量减少，在随后冷却中产生马氏体转变，使马氏体中碳含量呈递减趋势，因而硬度也逐渐降低[7]．在保证不出现裂纹的条件下，选择合适的氩弧重熔参数，用氩弧重熔方法制备的这种材料具有组织上的梯度过渡特点，能够带来性能上的渐变，并且涂层中不易出现富 Al 相，因而综合力学性能较好．

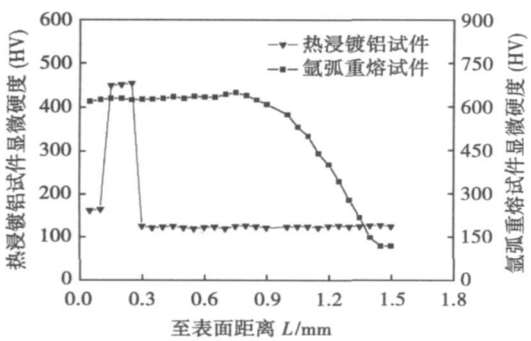

图 5　氩弧重熔前后显微硬度曲线

Fig. 5　Curves of hardness by TIG remelting pre- and post

2.3　氩弧重熔工艺参数对硬化效果的影响

2.3.1　焊接电流对裂纹率的影响

当焊接速度 $v=300$ mm/min，电弧电压 $U=10$ V，不同焊接电流下氩弧重熔处理热浸镀铝层的裂纹率测试结果见表 1．由表可见，随焊接电流增加，重熔层裂纹率下降．这是由于焊接电流增加时，热输入增加，重熔层应力减小，从而使裂纹率下降[7]．

表 1　不同焊接电流下的裂纹率

Table 1　Crack rates under difference welding currents

焊接电流 I/A	裂纹率 N/条
60	10.2
70	9.0
80	无
90	无
100	无

2.3.2　焊接电流对重熔层表面硬度及深度的影响

当焊接速度 $v=300$ mm/min，电弧电压 $U=10$ V 时，测得焊接电流与重熔层表面硬度、深度之间关系如图 6 所示．

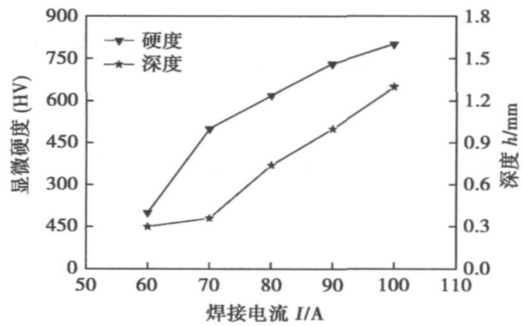

图 6　焊接电流对重熔层表面硬度和深度影响

Fig. 6　Influence of welding current on surface hardness and depth of remelting layer

由图 6 可见，随焊接电流增加，重熔层表面硬度、深度均增加．因为随焊接电流增加，单位面积氩弧热输入也随之增加，熔体量增多，使重熔层深度增加，也使得在极短时间内重熔层中相互扩散更为均匀混合，而激冷效果相对减小，使 Fe-Al 化合物能够形核、析出，故硬度升高．

2.3.3　焊接速度对重熔层裂纹率的影响

当焊接电流 $I=80$ A，电弧电压 $U=10$ V，不同焊接速度下氩弧重熔处理热浸镀铝层裂纹率测试结果见表 2．由表可见，随焊接速度增加，重熔层裂纹率增加．这是由于随焊接速度的增加，单位面积热输入减少，熔体量变小，基体对熔池的激冷作用增大，从而增加了重熔层内应力，导致裂纹逐渐增多．

表 2 不同焊接速度下的裂纹率

Table 2 Crack rates under difference welding speeds

焊接速度 v/(mm·min^{-1})	裂纹率 N/条
180	无
240	无
300	无
360	3.4
420	7.8

2.3.4 焊接速度对重熔层表面硬度及深度的影响

当焊接电流 I=80 A，电弧电压 U=10 V 时，测得焊接速度与重熔层表面硬度、重熔层深度之间的关系如图 7 所示.

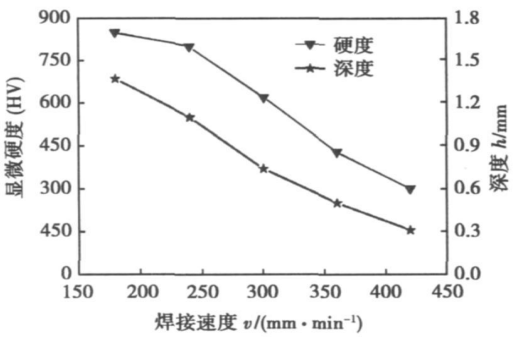

图 7 焊接速度对重熔层表面硬度和深度影响

Fig. 7 Influence of welding speed on surface hardness and depth of remelting layer

由图 7 可见，随焊接速度的增加，重熔层表面硬度降低，重熔层深度减小. 这是因为随焊接速度增加，氩弧热输入减小，熔池内液态金属在高温停留时间变短，冷却速度加快，导致重熔层深度变浅，重熔层内中相互扩散速度降低，Fe-Al 化合物来不及形核、析出，故硬度降低.

3 结 论

(1) 热浸镀铝层经氩弧重熔处理后，分层现象消失，组织上梯度过渡，试件由重熔层和淬硬层及基体构成. 重熔层由 Al，Fe，Fe_3Al 和 $FeAl_3$ 相组成，淬硬层组织为马氏体＋残留奥氏体.

(2) 氩弧重熔处理能明显提高热浸镀铝层的显微硬度. 重熔层硬度值最高可达 620 HV，淬硬层硬度下降缓慢，直至基体.

(3) 氩弧重熔工艺参数对重熔层深度、硬度和裂纹率影响较大，焊接电流增加或焊接速度减小时，重熔层深度增加，硬度升高，裂纹率下降.

参考文献：

[1] 于升学，夏 原，姚 枚. 扩散处理热浸镀铝钢高温抗氧化行为的研究[J]. 稀有金属材料与工程，2006，35(2)：74－78.
Yu Shengxue，Xia Yuan，Yao Mei. The oxidation resistance behavior of aluminized steel at high temperature in air after diffusion treatment [J]. Rare Metal Materials and Engineering，2006，35(2)：74－78.

[2] Grum J，Kek T. The influence of different conditions of laserbeam interaction in laser surface hardening of steels[J]. Thin Solid Films，2004，453－454(1)：94－99.

[3] Blednova Zh M，Budrevich D G，Makhutov N A. Deposition of coatings with the shape memory effect on the surface of steels by argon-arc facing[J]. Metal Science and Heat Treatment，2003，45(11－12)：428－431.

[4] 赵 霞，梁维中，徐家文，等. 球铁浸镀微弧氧化陶瓷层的制备与组织分析[J]. 表面技术，2008，37(2)：16－17.
Zhao Xia，Liang Weizhong，Xu Jiawen，*et al*. The preparation and the microstructure of the ceramic coating of HDA and microarc oxidation[J]. Surface Technology，2008，37(2)：16－17.

[5] Tomida S，Nakata K. Fe-Al composite layers on aluminum alloy formed by laser surface alloying with iron powder[J]. Surface and Coatings Technology，2003(174－175)：559－563.

[6] 李殿凯，袁晓敏. 5CrNiMo 热浸镀铝激光重熔层组织观察[J]. 兵器材料科学与工程，2007，30(1)：11－13.
Li Diankai，Yuan Xiaomin. Microstructure observation of coating prepared by hot-dipped aluminum and laser remelting on the surface of 5CrNiMo[J]. Ordnance Material Science and Engineering，2007，30(1)：11－13.

[7] 杨 莉，肖 龙，娄高峰. 氩弧硬化对硼铸铁表面组织和性能的影响[J]. 金属热处理，2007，32(3)：69－71.
Yang Li，Xiao Long，Lou Gaofeng. Influence of argon arc hardening process on microstructure and properties of boron cast iron surface[J]. Heat Treatment of Metals，2007，32(3)：69－71.

作者简介：赵 霞，女，1980 年出生，硕士，讲师. 主要从事热浸镀铝及氩弧重熔方面的科研和教学工作. 发表论文 7 篇.

Email：sunyxzhaox@163.com

ner. The maximum stress of PBGA121 soldered joints increases when chip size increases, while the maximum stress of PBGA81 soldered joints decreases first and then increases. Based on the modified Manson-Coffin model by Engelmaier, the fatigue lives of critical soldered joints conditions corresponding to four different chip sizes were predicted, and it is found that the size of Silicon chip has a significant effect on the fatigue life of soldered joints.

Key words: plastic ball grid array; arrangement model; chip size; fatigue life

Realization of high-speed DPWM controller in all-digital inverter based on FPGA DUAN Bin, SUN Tongjing, LI Zhenhua, MEI Gaoqing (School of Control Science and Engineering, Shandong University, Jinan 250061, China). p 77—80

Abstract: A digital pulse width modulation (DPWM) controller was researched and designed based on field programmable gate array (FPGA). And a new method was also presented to produce PWM driving signals in all-digital inverter. The real-time counting comparative method was introduced to realize high frequency PWM signals with adjustable frequency and duty cycle, which can realize that every moment of the PWM signals is knowable and controllable. Every block of the controller was described in detail after analysis of principles and parameters of the DPWM controller. The digital anti-jamming technology was adopted to make the system work steadily in the terrible environment with strong disturbance, high voltage and large current. The simulation and actual welding experiments demonstrate that the high-speed DPWM controller can run steadily and reliably in a long time and be widely used in the digital welding machines.

Key words: all-digital inverter; FPGA; PWM controller; high frequency inverter

Experiment on tensile and shear strength of front fillet welded joint post-high-temperatures CHEN Jianfeng[1,2], CAO Pingzhou[1], DONG Xianfeng[1] (1. College of Civil Engineering, Hehai University, Nanjing 210098, China; 2. School of Civil Engineering, Chang'an University, Xi'an 710061, China). p 81—84

Abstract: In order to investigate the characteristics of tensile and shear strength of front fillet welded joint post-high-temperatures, the tension tests for double strapped front fillet welded joint were conducted after cooling down from different high temperatures. The tests indicate that specimens are fractured at the middle of steel plate as the maximum temperature undergone below 500 ℃ and brittle fractured at the throat of fillet weld as the maximum temperatures undergone above 500 ℃. The maximum temperature undergone and the cooling pattern are major factors influencing tensile and shear strength of front fillet welded joint post-high-temperatures. Based on the experimental results, this paper proposes the calculation formulas of tensile and shear strength of front fillet welded joint post-high-temperatures. The conclusions supply references for evaluation damage and reinforcement of steel structure post fire.

Key words: front fillet welded joint; post-high-temperatures; tensile and shear strength; experiment

Robust joint recognition with structured-light vision sensing GONG Yefei, DAI Xianzhong, LI Xinde (Key Laboratory of Measurement and Control of Complex Systems of Engineering, Southeast University, Nanjing 210096, China). p 85—88

Abstract: A model-based method is proposed for recognition of weld joints composed of line segment features. Shape features of the structured-light stripe centerline are extracted sequentially by calculating the peak mass position of gray distribution for the image columns and fitting the piecewise line segments using the least squares method, then stripe profile is described qualitatively by predefined primitive labels, and lastly a hypothesize-verification based model matching algorithm is implemented to recognize the joint. During the matching, undetected portion of joint profile, due to optical noises such as welding spatters, secondary reflection, tack weld, and other unexpected imaged sources, can be recovered to ensure the correct recognition results by merging profile's primitives and reconstructing the relations with the top-level heuristic knowledge of the joint models. Experiments show, even in a cluttered environment with different disturbances, correct results can be acquired by combining top-level model and bottom-level data.

Key words: weld joint; structured-light; pattern recognition; model matching

Deviation extraction for through-arc sensor with sinusoidal weave motion GAN Yahui, DAI Xianzhong (Key Lab of Measurement and Control of CSE, Ministry of Education, Southeast Universing, Nanjing 210096, China). p 89—92

Abstract: A new algorithm to extract the weld torch lateral deviation for through-arc sensor with sinusoidal weave motion was proposed in this paper. Based on the detailed analysis of the welding current waveform in through-arc sensor with sinusoidal weave motion, the lateral deviation expression was deducted following the left-right area difference method. Adopting the function approximation theory, an index related to the lateral deviation was defined and the optimum result was calculated under this least mean square index. Experimental result proved the validity of the proposed algorithm. These results established the foundation for applications of the through-arc sensor in seam tracking system.

Key words: through-arc sensor; sinusoidal weave motion; deviation extraction; least mean square approximation; seam-tracking

Influence of argon arc remelting process on microstructure and properties of coating prepared by hot dipping aluminizing on surface Q235 steel ZHAO Xia[1], XU Jiawen[1], SUN Yongxin[2] (1. School of Materials Science and Engineering, Heilongjiang University of Science and Technology, Harbin 150027, China; 2. Harbin Institute of Large Electrical Machinery, Harbin Electric Machinery Company Limited, Harbin 150040, China). p 93—96

Abstract: Surface modification was carried out on hot dipping aluminizing surface of Q235 steel by argon arc remelting technology. The preand post microstructure steel treated by the argon arc remelting was investigated using SEM and XRD, the preand post microhardness of specimen cross section by argon arc remelting was also

determined. Effect of argon arc remelting parameters on microstructure and mechanical properties of hot dipping aluminizing surface was investigated. The results show that, for the hot dipping aluminizing coating after argon arc remelting treatment, stratification phenomenon disappeared, gradient transition on microstructure appeared, specimen consisted of remelting layer, transition layer and substrate. Argon arc remelting treatment can obviously increase microhardness of hot dipping aluminizing coating. The process parameters influence the depth, hardness and crack rate of the remelting layer markedly. With the welding current increasing or the welding speed decreasing, the remelting layer depth and hardness increases, and the crack rate decreases.

Key words: hot dipping aluminizing (HDA); argon arc remelting; microstructure; microhardness

Simulation of viscoelastic heat during ultrasonic welding of thermoplastics ZHANG Zhenqiang[1], ZHANG Zongbo[1], LUO Yi[1,2], WANG Xiaodong[1,2], WANG Liding[1,2] (1. Key Laboratory for Precision and Non-traditional Machining Technology of Ministry of Education, Dalian University of Technology, Dalian 116024, Liaoning, China; 2. Key Laboratory for Micro/Nano Technology and System of Liaoning Province, Dalian 116024, Liaoning, China). p 97—100

Abstract: Viscoelastic heat is one of the main heat sources during ultrasonic welding of thermoplastics. Unfortunately the present works could not definitely take into account the dynamic viscoelasticity of thermoplastics. In this paper a simplified method was proposed to characterize dynamic viscoelasticity based on static relaxation modulus and TTEP (time-temperature equivalent principle). The method could represent dynamic modulus as the function of temperature and frequency, and avoids calculating dynamic modulus of high frequency by shifting and extrapolating the dynamic modulus of lower frequency from experiments. With the method mentioned above, a strategy was put forward to simulate the viscoelastic heat of PMMA (polymethyl methacrylate) under periodic load using FEM (finite element method). The calculated temperature shows a similar tendency as tested results in other literatures.

Key words: ultrasonic welding; dynamic viscoelasticity; viscoelastic heat; finite element method

Joints performance of diffusion bonding between pure Cu and stainless steel and dynamic analysis of atomic diffusion LIU Shuying (Key laboratory of Advanced Non-ferrous Metals, Henan University of Science and Technology, Luoyang 471003, Henan, China). p 101—104

Abstract: The effects of welding parametas on the performance of the joints of pure copper and ferrite 410L and joints of pure copper and austenite 304 stainless steel were researched by microstruture observation, hardness, tensile test and EPMA. And atomic diffusion mechanism of two kinds of joints combined theoretical calculation was also discussed. The result indicated: as bonding pressure and bonding time fixed, the joints tensile strength increased with the bonding temperature. Optimal bonding temperature of Cu/410L is about 50 K lower than that of Cu/304, because the diffusion speed of Cu, bcc ferrite is faster than in fcc austenitic. The measured diffusion speed of Cu atom in stainless steel is smaller than the theoretical value because the theoretical value was obtained based on assuming 100% full adhesion for the surface in initial, but the actual bonding surface is rough in initial stages.

Key words: diffusion bonding; diffusion speed; ferritic; austenitic; tensile strength

Microstructure and properties of 65Mn spring steel by laser welding LIU Qibin, LI Bin (Materials School of Guizhou University, Caijiaguan Branch, Guiyang 550003, China). p 105—108

Abstract: To obtain excellent welding joint, 65Mn spring steel was welded by 5 kW CO_2 laser welding equipment. Microstructure, tensile strength, tensile fracture and residual stress of this joint were investigated by means of OM, XRD, SEM, microhardness testing machine, electronic universal testing machine and residual stress test machine. The experimental results indicate that the fine equiaxised crystal, dendrite crystal and cell grain are formed from welding central zone to edge zone, respectively. In the HAZ, the over-heated zone is mainly comprised of coarse acicular martensite. Recrystalline zone mainly consistes of fine acicular martensite. The part transforming zone is comprised of ferrite and pearlite. The welding joint mainly consists of fine α-Fe, Fe_3C and FeSi. The highest hardness value of welding zone and HAZ is 720 HV and 770 HV, respectively. The hardness decreases significantly from HAZ to base metal. The average tensile strength of welding joints is approximately 475 MPa. The average residual stress in welding zone is 105 MPa, and the average residual stress in HAZ is —60 MPa.

Key words: spring steel; 65Mn; laser welding; microstructure; properties

Prediction for welding deformation reducing by welding sequence optimization of upper plate ZHOU Guangtao[1,2], LIU Xuesong[2], YAN Dejun[2], FANG Hongyuan[2] (1. College of mechanical Engineering and Automation, Huaqiao University, Xiamen 361021, China; 2. State Key Laboratory of Advanced Welding Production Technology, Harbin Institute of Technology, Harbin 150001, China). p 109—112

Abstract: The numerical simulation of welding deformation of upper plate structure for large-scale crane box beam was conducted using the thermo elastic-plastic method. Analysis model was established to quantitatively describe the effects of welding sequence for both longitudinal rib to upper plate and transverse rib to upper plate on welding deformation. The optimal welding sequence of the whole structure was obtained by the term of the "and" relation. The simulation value of deformation under the optimal welding sequence was contrast to measured value to show the better agreement for two values. The deformation of the optimal sequence and the worst sequence was 15.12 mm and 28.47 mm, respectively.

Key words: numerical simulation; welding sequence; optimal; prediction